Supplementary Information Associated with

Unraveling the therapeutic potentials of a thiosemicarbazone based Zn(II) metal-organic triangle complex

Ansa Santu[a], K. Sreekanth[b,c], M.K. Sarath Josh[d], E.K. Radhakrishnan[b,c], E. Manoj[a]*

[a]*Department of Applied Chemistry, CUSAT, Kochi, Kerala 682 022, India*
[b]*School of Biosciences, Mahatma Gandhi University; P.D Hills (P.O), Kottayam, Kerala 686 560, India*
[c]*Dr. N. Radhakrishnan International Centre for Medical Innovation (NRICMI), Mahatma Gandhi University; P.D Hills (P.O), Kottayam, Kerala 686 560, India*
[d]*School of Energy Materials, Mahatma Gandhi University; P.D Hills (P.O), Kottayam, Kerala 686 560, India*

Email: *manoje@cusat.ac.in

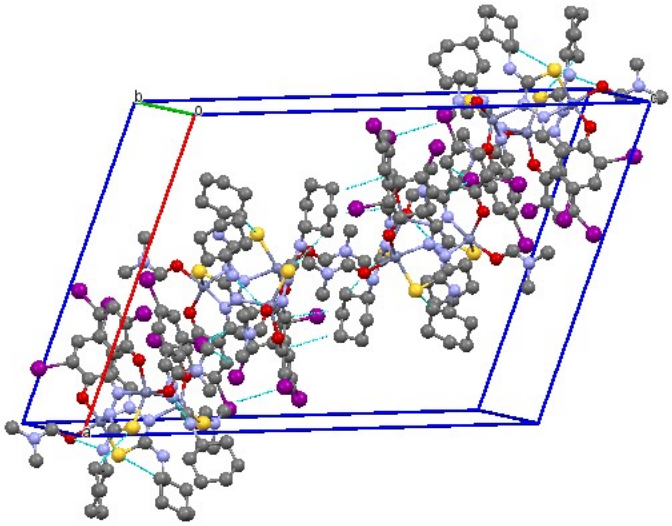

Figure S1. Packing diagram of complex **1** along the b-axis showing hydrogen bonding interactions.

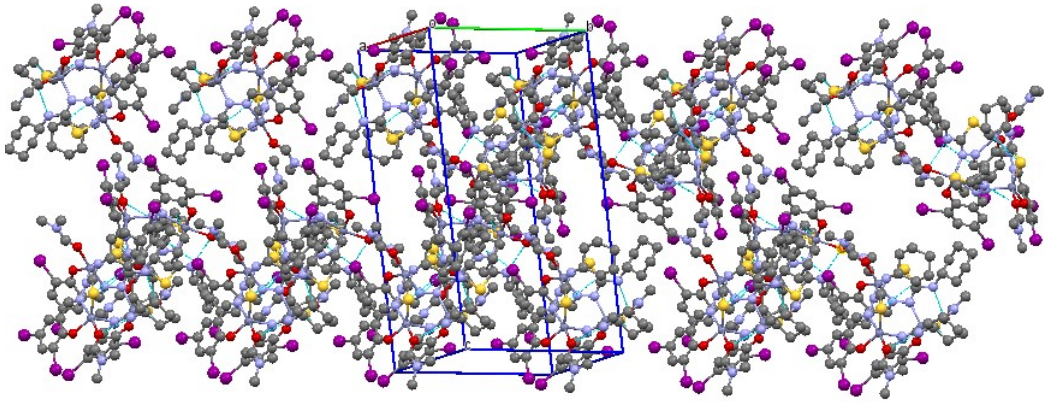

Figure S2. Packing of complex **1** showing molecules are packed along the a-axis and the formation of 3D motif through hydrogen bonding and other short contacts.

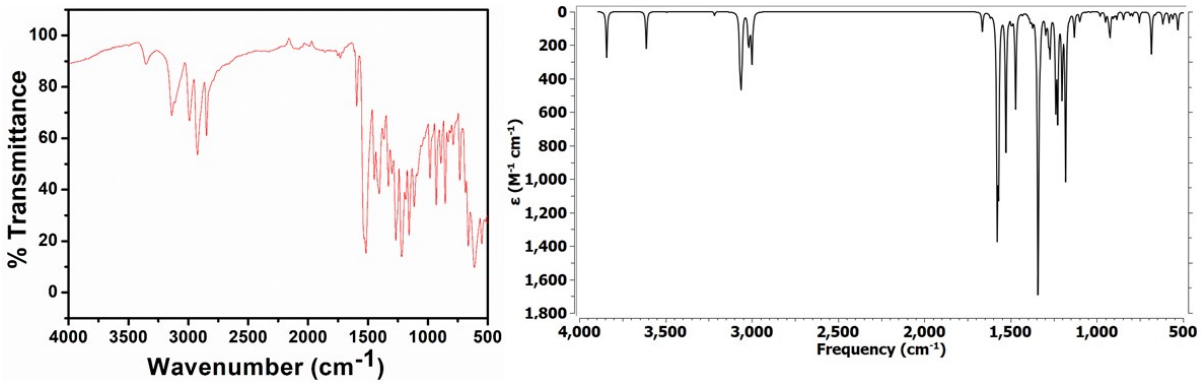

Figure S3. Experimental (left) and theoretical (right) IR spectra of the ligand H_2L.

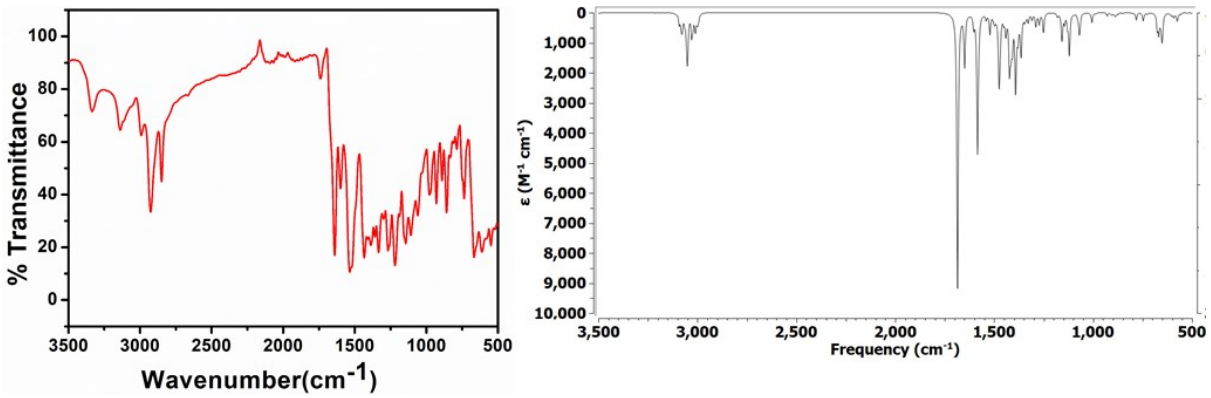

Figure S4. Experimental (left) and theoretical (right) IR spectra of the complex **1**.

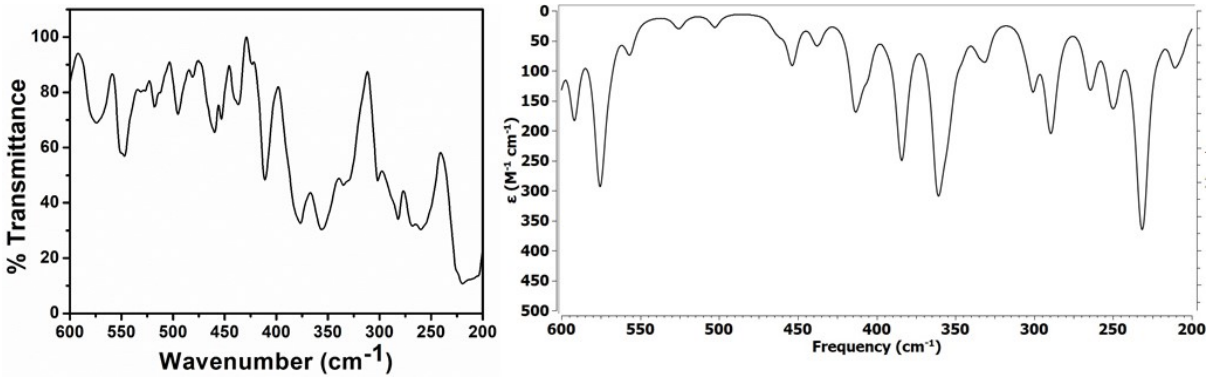

Figure S5. Experimental (left) and theoretical (right) Far IR spectra of the complex **1**.

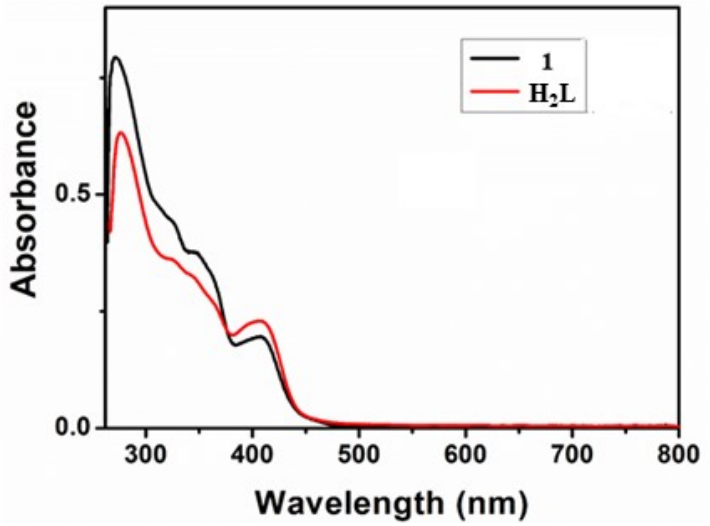

Figure S6. UV-vis spectra of ligand H_2L and the complex **1** in 10^{-5} M DMF solution.

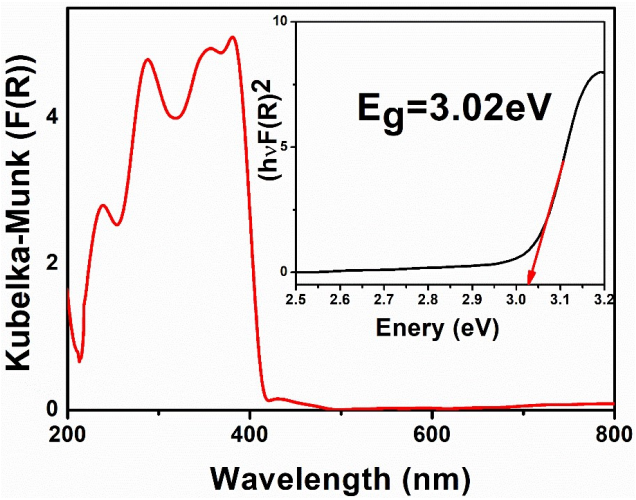

Figure S7. UV-vis diffuse reflectance spectrum of H_2L. Inset shows the band gap calculations.

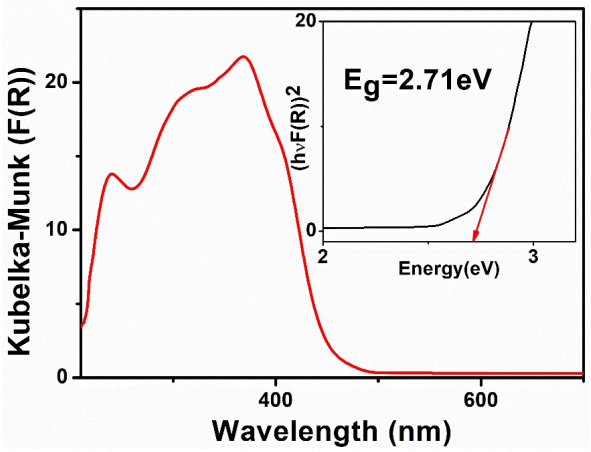

Figure S8. UV-vis diffuse reflectance spectrum of complex **1**. Inset shows the band gap calculations.

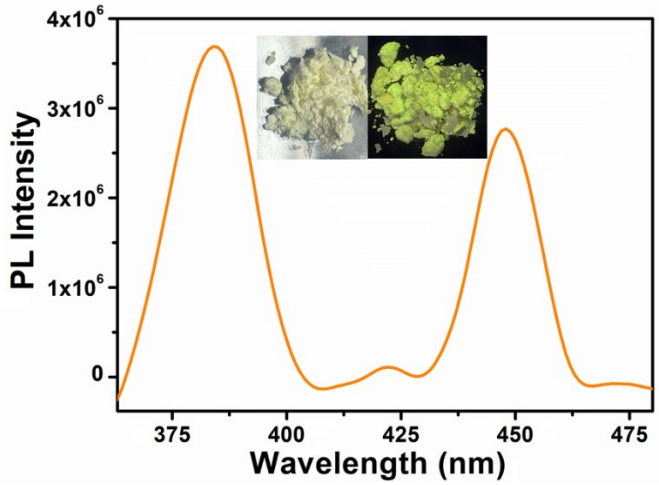

Figure S9. Solid state emission spectrum of H_2L (λ_{exc} = 307 nm). Inset shows the photographs under daylight and UV light.

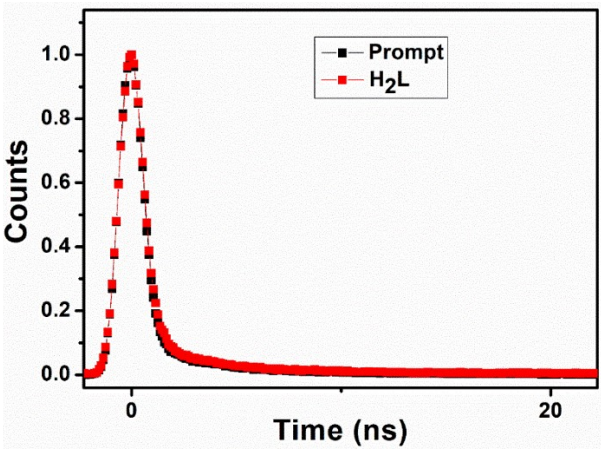

Figure S10. Time resolved fluorescence decay curve of the ligand H_2L.

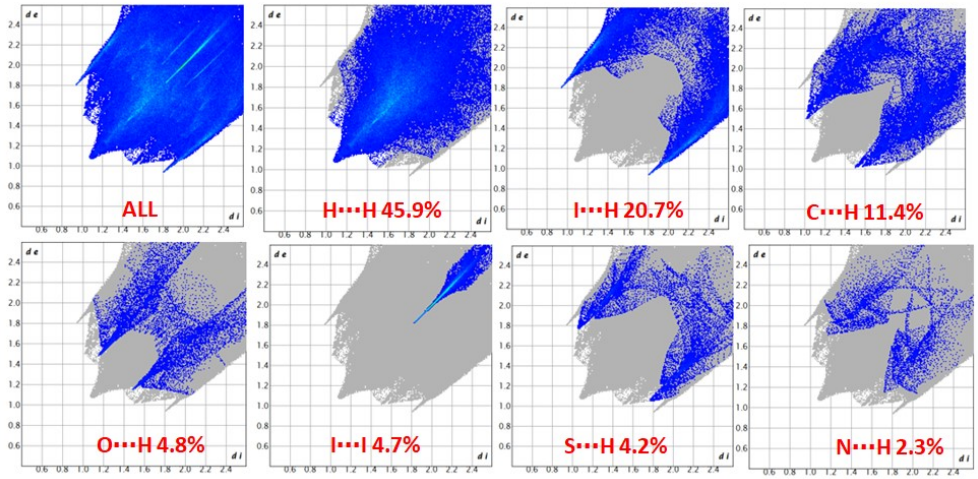

Figure S11. 2D Fingerprint plots showing the percentages of contacts contributed to the total Hirshfeld surface area of the complex **1**.

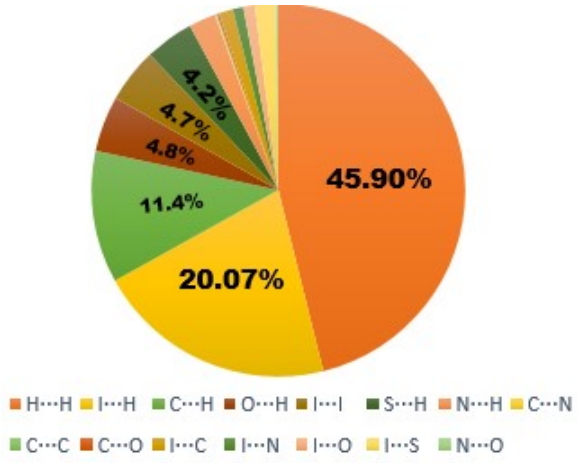

Figure S12. Relative contributions of various intermolecular contacts to the Hirshfeld surface area in complex **1**.

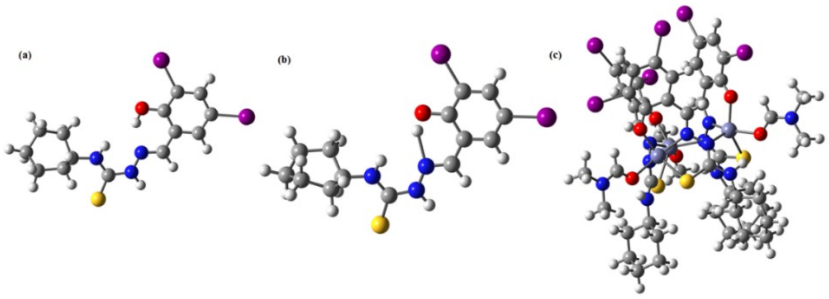

Figure S13. Optimized geometries of (a) H_2L, (b) H_2L-keto, (c) complex **1**.

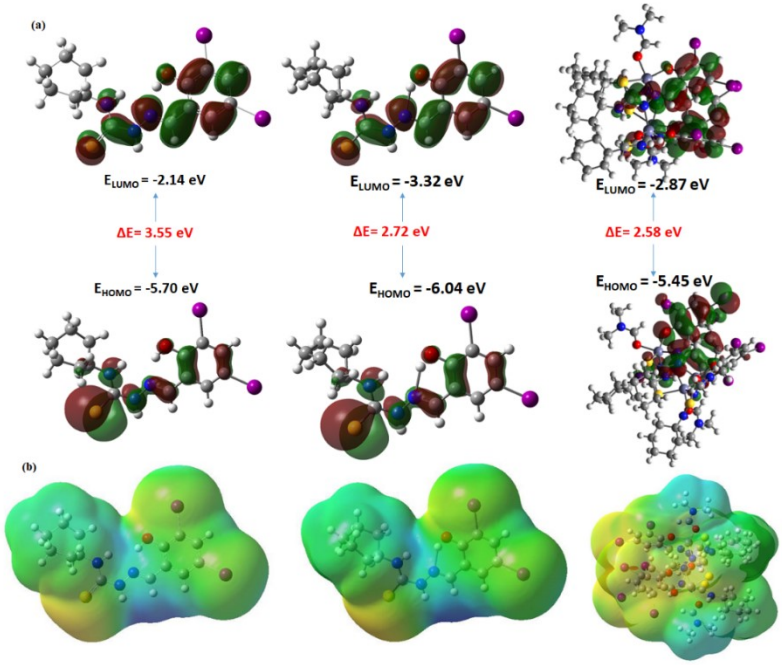

Figure S14. (a) Frontier molecular orbitals, (b) MEP plots of H_2L, H_2L-keto, complex **1**.

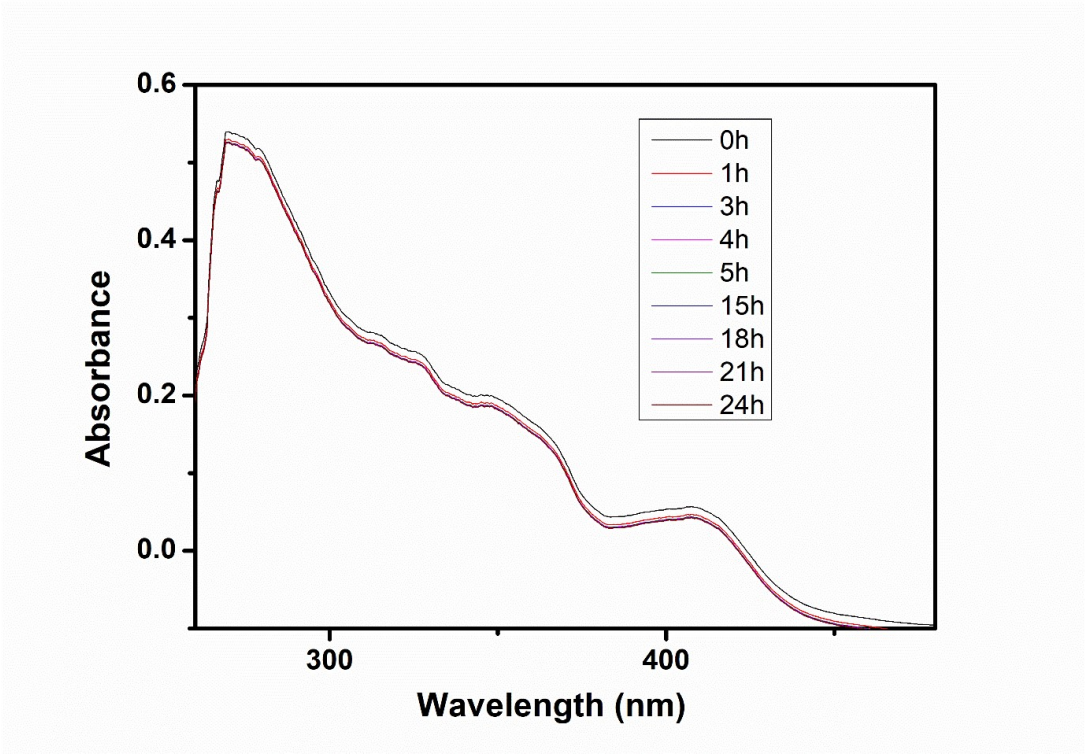

Figure S15. Time dependent absorption spectra of complex **1** in buffer solution at pH =7.4.

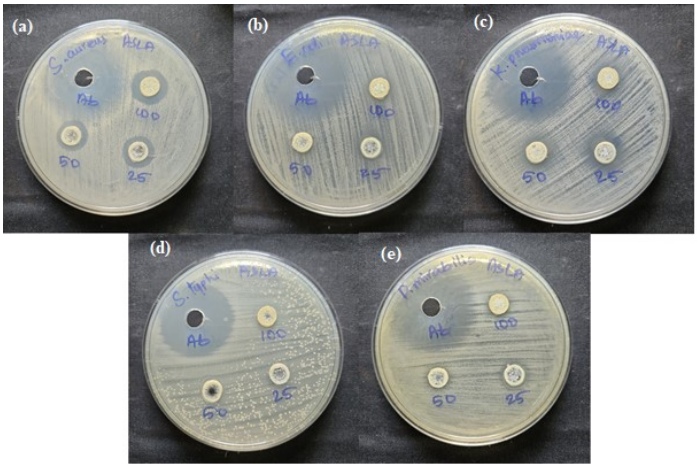

Figure S16. Zone of inhibition of the ligand H_2L against (a) *S. aureus*, (b) *E. coli,* (c) *K. pneumoniae,* (d) *S. typhi.* (e) *P. mirabilis*.

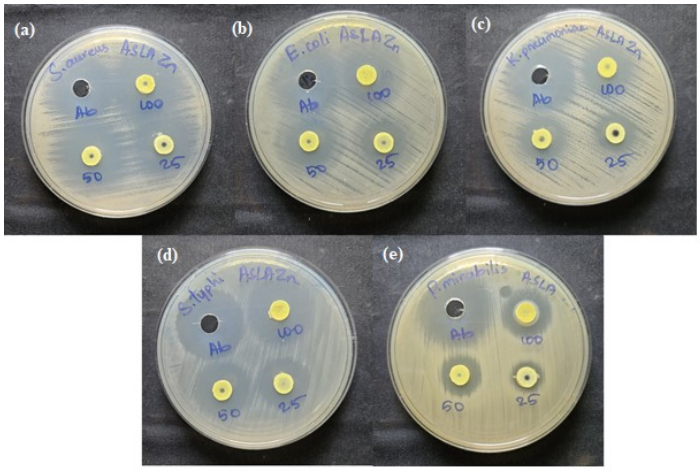

Figure S17. Zone of inhibition of the complex **1** against (a) *S. aureus*, (b) *E. coli,* (c) *K. pneumoniae,* (d) *S. typhi.* (e) *P. mirabilis*.

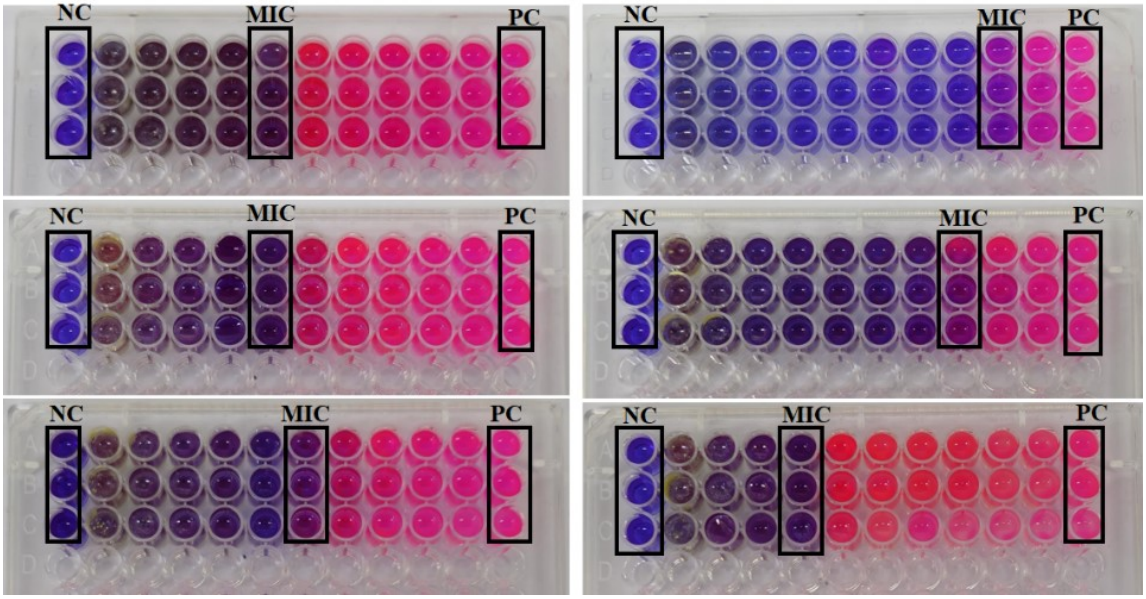

Figure S18. MIC determination against *S. aureus* of ligand H_2L (top left), complex **1** (top right), *E. coli* of complex **1** (middle left), *K. pneumoniae* of complex **1** (middle right), *S. typhi* of complex **1** (bottom left), *P. mirabilis* of complex **1** (bottom right).

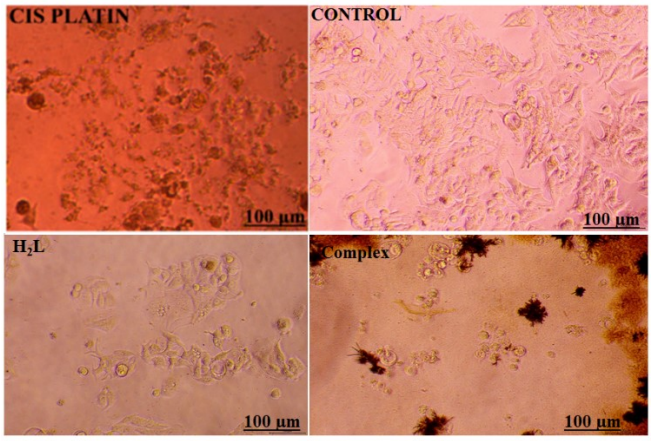

Figure S19. Morphological changes induced by H_2L and complex **1** against MCF7 cell lines compared with cisplatin at 100 µg/mL.

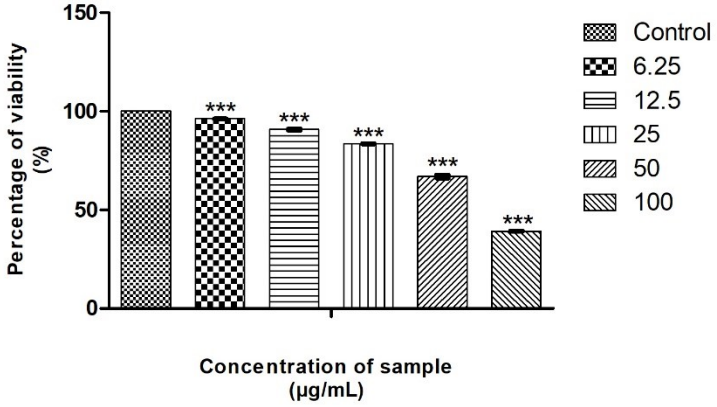

Figure S20. Assessment of HEK 293 cell survival in the presence of complex **1**, conducted by treating the cells with different concentrations. (*) indicate $p < 0.001$ when compared to control group.

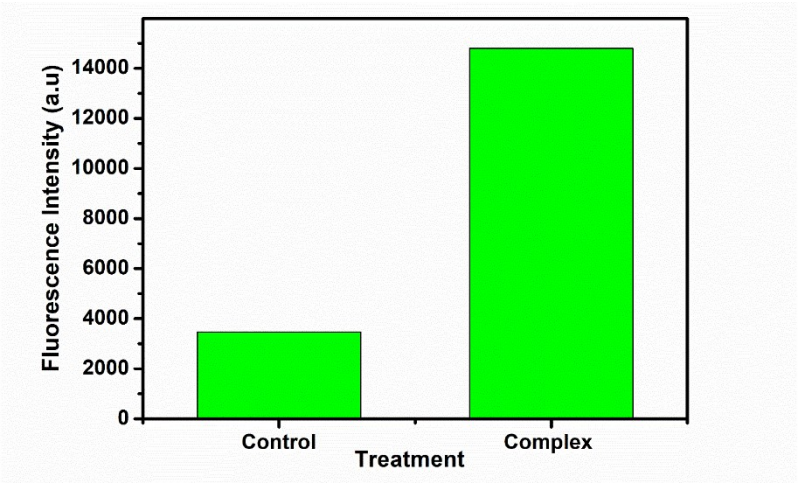

Figure S21. Fluorescent intensity plot of DCFDA/DCF assay performed for the detection of ROS generation in MCF7 cells by complex **1** compared with untreated control.

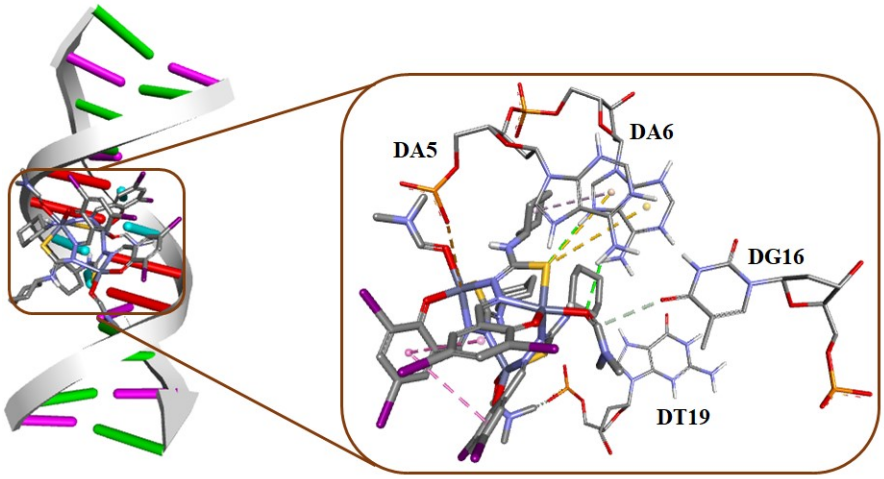

Figure S22. Binding mode of [Zn_3(μ-L)$_3$·3DMF] (**1**) and its focused view of interactions with 1BNA.

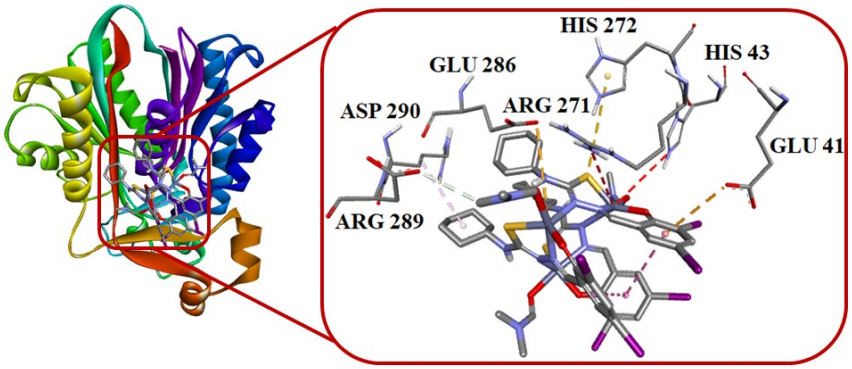

Figure S23. Binding mode of [Zn_3(μ-L)$_3$·3DMF] (**1**) and its focused view of interactions with 1HNJ.

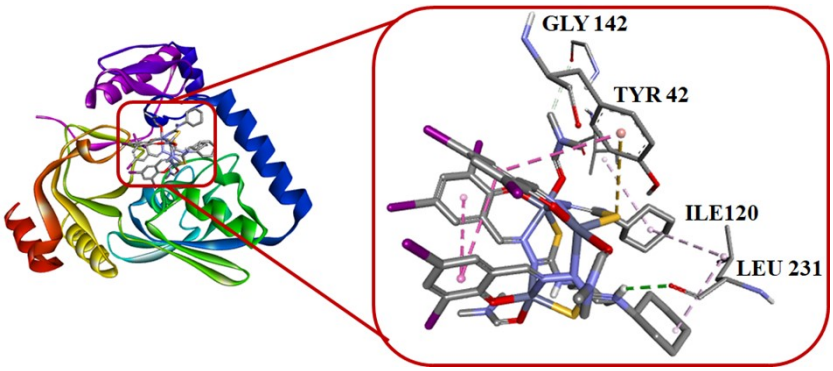

Figure S24. Binding mode of [Zn_3(μ-L)$_3$·3DMF] (**1**) and its focused view of interactions with 1HSK.

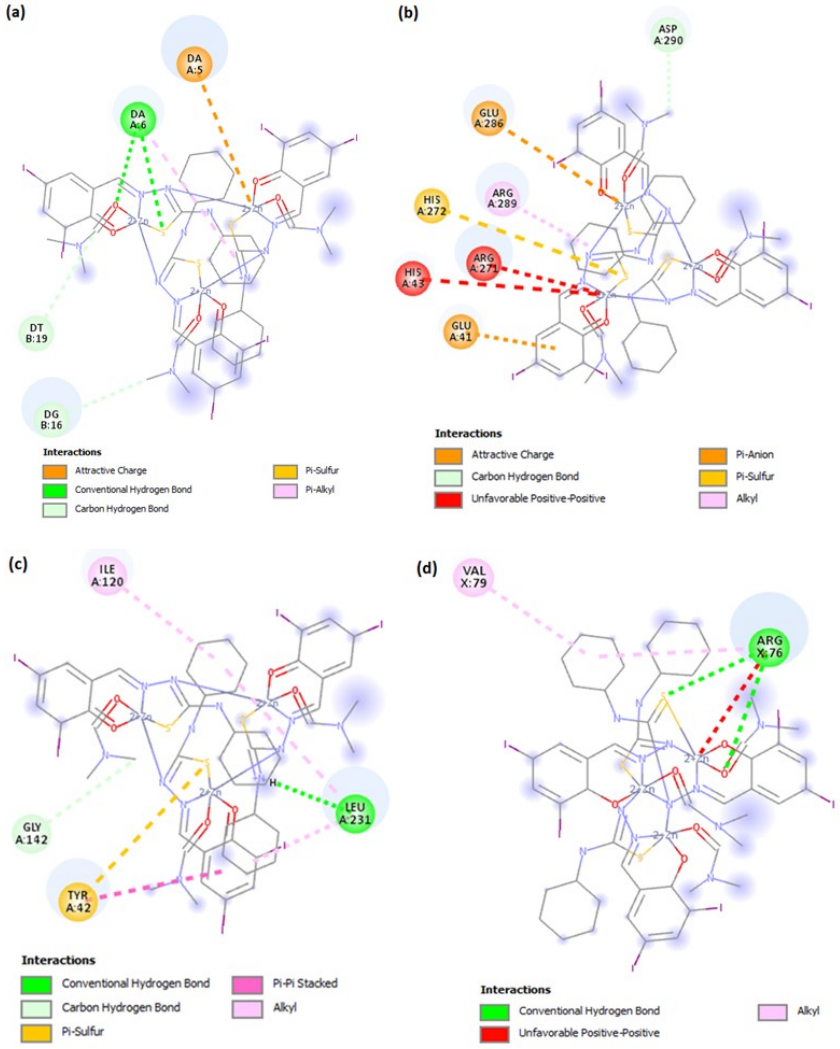

Figure S25. 2D representation of [Zn_3(μ-L)$_3$·3DMF] (1) with the active site residues of (a) 1BNA, (b) 1HNJ, (c) 1HSK and (d) 3HB5.

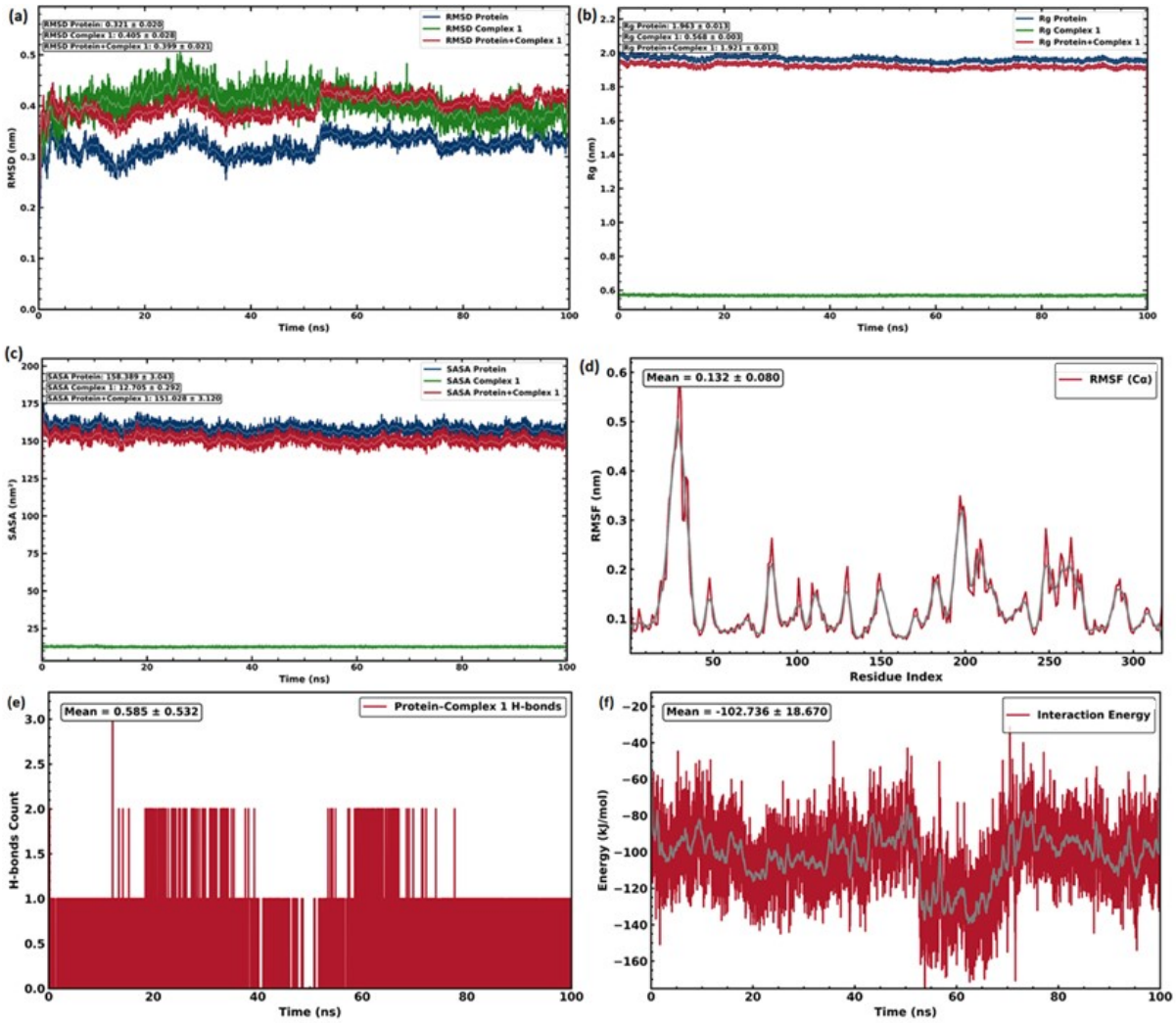

Figure S26. MD simulation profile of the Complex **1**-1HNJ system over 100 ns (a) RMSD (b) Rg (c) SASA (d) RMSF (e) hydrogen bonds (f) interaction energy.

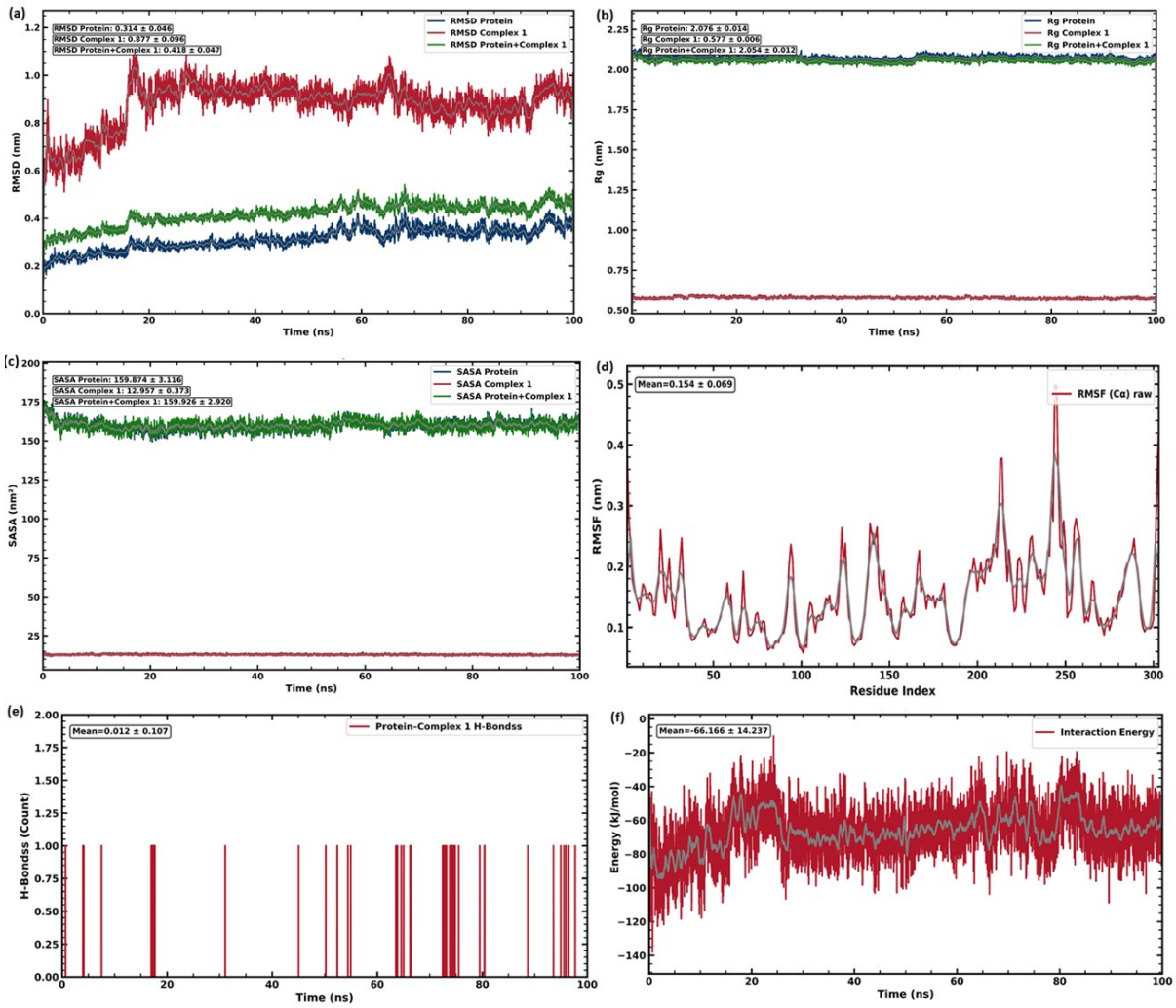

Figure S27. MD simulation profile of the Complex **1**-1HSK system over 100 ns (a) RMSD (b) Rg (c) SASA (d) RMSF (e) hydrogen bonds (f) interaction energy.

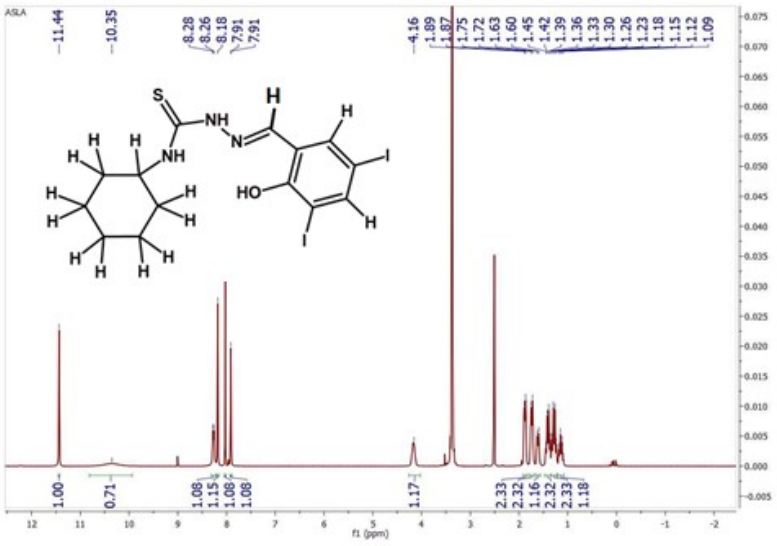

Figure S28. ^{1}H NMR spectrum of H_2L.

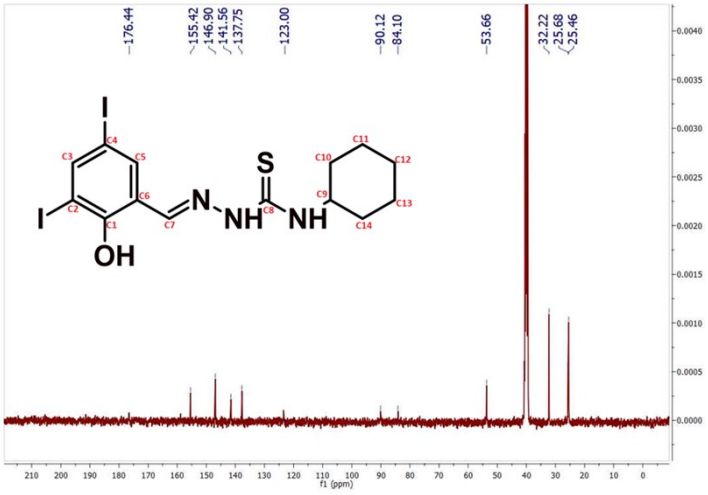

Figure S29. ^{13}C NMR spectrum of H_2L.

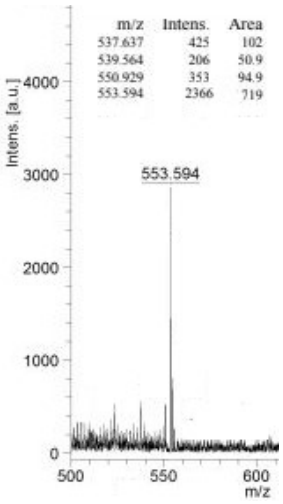

Figure S30. Mass spectrum of H_2L.

Table S1. The bond lengths (Å) and bond angles (˚) of the complex $[Zn_3(\mu\text{-}L)_3.3DMF]$ (**1**).

Bond lengths (Å)		Bond angles (˚)	
Zn(1)–N(2)	2.077(3)	O(2)–Zn(1)–N(2)	113.35(11)
Zn(1)–N(7)	2.106(3)	O(2)–Zn(1)–N(7)	87.59(11)
Zn(1)–S(2)	2.3229(10)	N(2)–Zn(1)–N(7)	100.01(12)
Zn(1)–O(2)	1.975(3)	O(2)–Zn(1)–O(6)	88.78(11)
Zn(1)–O(6)	2.179(3)	N(2)-Zn(1)-O(6)	93.34(11)
Zn(2)–O(3)	1.975(3)	N(7)-Zn(1)-O(6)	166.53(11)
Zn(2)–O(5)	2.120(3)	O(2)–Zn(1)–S(2)	139.09(8)

Zn(2)–S(3)	2.3551(10)	N(2)–Zn(1)–S(2)	107.44(9)
Zn(2)–N(8)	2.091(3)	N(7)–Zn(1)–S(2)	82.40(8)
Zn(2)–N(6)	2.130(3)	O(6)–Zn(1)–S(2)	91.94(8)
Zn(3)–O(4)	2.113(3)	O(3)–Zn(2)–N(8)	115.14(11)
Zn(3)–O(1)	1.983(3)	O(3)–Zn(2)–O(5)	90.43(11)
Zn(3)–S(1)	2.3545(10)	N(8)–Zn(2)–O(5)	92.79(11)
Zn(3)–N(1)	2.094(3)	O(3)–Zn(2)–N(6)	87.53(11)
Zn(3)–N(5)	2.096(3)	N(8)-Zn(2)-N(6)	98.49(12)
N(7)–N(8)	1.396(4)	O(3)-Zn(2)-S(3)	135.12(8)
N(6)–N(5)	1.395(4)	N(8)–Zn(2)–S(3)	109.31(9)
N(1)–N(2)	1.396(4)	O(5)–Zn(2)–S(3)	93.38(8)
S(1)–C(8)	1.740(4)	N(6)–Zn(2)–S(3)	80.07(8)
S(2)–C(36)	1.737(4)	O(5)–Zn(2)–N(6)	168.32(11)
S(3)–C(22)	1.744(4)	O(1)–Zn(3)–N(1)	87.19(11)
C(8)–N(2)	1.336(5)	O(1)–Zn(3)–N(5)	116.55(12)
N(5)–C(22)	1.337(5)	N(1)–Zn(3)–N(5)	97.96(12)
N(8)–C(36)	1.345(5)	O(1)–Zn(3)–O(4)	89.93(10)

Table S2. Interaction parameters of the complex [Zn_3(μ-L)$_3$.3DMF] (**1**).

Hydrogen bonding interactions				
D–H ··· A	D–H (Å)	H ··· A (Å)	D--A (Å)	D–H ··· A (°)
N3–H3A ··· O6	0.84(4)	2.17(4)	2.959(5)	156(4)
N4–H4A ··· O4	0.84(5)	2.46(6)	3.316(5)	138(5)
N9–H9A ··· O5	0.85(3)	2.16(3)	2.957(5)	157(4)
C7–H7 ··· O2	0.95	2.40	3.294(4)	157
C9–H9 ··· S1	1.00	2.65	3.060(4)	105
C21–H21 ··· O1	0.95	2.50	3.348(5)	149
C35–H35 ··· O3	0.95	2.46	3.352(5)	157
C42–H42B ··· S2	0.99	2.76	3.365(4)	120
C43–H43 ··· O2	0.95	2.33	2.942(5)	122
C44–H44A ··· I1[a]	0.98	2.86	3.837(4)	177
C44–H44B ··· I6[a]	0.98	2.86	3.819(4)	166
C46–H46 ··· O3	0.95	2.48	3.042(5)	118
C49–H49 ··· O1	0.95	2.33	2.935(5)	121

D = donor, A = acceptor, Equivalent position codes a = x,1-y,2-z.

C–X ··· π interactions			
C–X ··· Cg	X ··· Cg (Å)	C ··· Cg (Å)	C-X ··· Cg (°)
C5–H5 ··· Cg(11)[a]	2.78	3.629(4)	150
C15–H15 ··· Cg(7)[a]	2.87	3.594(4)	134
C29–H29 ··· Cg(9)[a]	2.95	3.742(4)	141

Equivalent position codes: a= x,y,z; Cg(7)= C(1), C(2), C(3), C(4), C(5), C(6); Cg(9)= C(15), C(16), C(17), C(18), C(19), C(20); Cg(11)= C(29), C(30), C(31), C(32), C(33), C(34).

Table S3. The Frontier molecular orbital energies and calculated chemical reactivity parameters for the ligand and complex.

Energy parameters (eV)	**H_2L**	**H_2L-keto**	**1**
HOMO	-5.70	-6.04	-5.45
HOMO-1	-5.95	-6.25	-5.95
LUMO	-2.14	-3.32	-2.87
LUMO+1	-1.48	-1.36	-1.48
E_{HOMO}–E_{LUMO}: ΔE	3.55	2.72	2.58
Ionization Energy, I	5.70	6.04	5.45
Electron Affinity, A	2.14	3.32	2.87
Chemical hardness, η	1.78	1.36	1.29
Electronegativity, χ	3.92	4.68	4.16
Chemical potential, μ	-3.92	-4.68	-4.16
Electrophilicity, ω	4.31	8.05	6.70
Total Energy	-32772.12	-32804.77	-123877.59
Global softness, σ (eV^{-1})	0.56	0.73	0.77
Nucleophilicity, ε (eV^{-1})	0.23	0.12	0.12
Dipole moment (Debye)	8.20	4.99	12.07

Table S4. Results of the inhibitory zones of the ligand and complex **1**.

Compounds	Zone of Inhibition (mm)				
	S. aureus	*E. coli*	*S. typhi*	*K. pneumoniae*	*P. mirabilis*
H_2L	17±1	11±1	0	11.33±1.52	0
1	33±1.73	23±1	26.67±1.53	23±1	20.67±1.53
Ciprofloxacin	27.33±0.57	29.67±0.57	27.67±1.15	32±1	29.33±1.52

Table S5. The percentage of cell viability of MCF-7 cell with the concentrations of ligand H_2L and complex **1**.

Samples	Concentration (μg/mL)	Average Absorbance @ 540 nm	% Cell Viability
		MCF-7	MCF-7
H_2L	Control	0.5766	100
	6.25	0.5561	96.44
	12.5	0.4686	81.26
	25	0.3782	65.59
	50	0.3098	53.73
	100	0.2467	42.79
	6.25	0.4800	83.25
	12.5	0.48087	70.88

Complex 1	25	0.2373	41.15
	50	0.1772	30.73
	100	0.1096	19.01

Table S6. Physicochemical properties and in silico ADMET profile of **1**.

Properties	Complex **1**
Physicochemical and medicinal properties	
MW	1996.84
TPSA	581.945
$LogP_{o/w}$	11.064
Absorption	
Caco-2 Permeability	0.78
HIA	85.25
P-gp substrate	0.869
Distribution	
BBB	-2.923
FU	0.394
Metabolism	
CYP3A4 inhibitor	1(yes)
Excretion	
CL_{plasma}	-34.217
Toxicity	
Human hepatotoxicity (H-HT)	No

Note. **MW**: molecular weight (≤500 g/mol), **TPSA**: topological polar surface area (Å^2), **LogP**: logarithm of partition coefficient (≤5) of compound between n-octanol and water, **HIA**: Human intestinal absorption (HIA+<30%<HIA-), **P-gp**: P-glycoprotein inhibitor/ substrate (0 to 0.3, excellent; 0.3 to 0.7, medium; 0.7 to 1.0, poor), **BBB**: Blood-Brain Barrier penetration (~1: BBB+;~0: BBB-), **FU**: Fraction unbound in plasmas (Low; <5%, Middle; 5~20%, High; > 20%), **CYP3A4 inhibitor**: Cytochrome P450 monooxygenase enzyme (~1; inhibitor, ~0; non-inhibitor), **CL_{plasma}**: ml/min/kg. >15 ml/min/kg; high clearance, 5-15 ml/min/kg; moderate clearance, < 5 ml/min/kg; low clearance, **H-HT**: Human hepatotoxicity (0 to 0.3, low; 0.3 to 0.7, medium; 0.7 to 1.0, high).